https://doi.org/10.22226/2410-3535-2020-2-217-222 PACS: 62.20-x, 62.20 me

Effect of deformation processing of the dilute Mg-1Zn-0.2Ca alloy on the mechanical properties and corrosion rate in a simulated body fluid

D. L. Merson[†,1], A. I. Brilevsky[1], P. N. Myagkikh[1], M. V. Markushev[2], A. Vinogradov[3]

[†]d.merson@tltsu.ru

[1]Institute of Advanced Technologies, Togliatti State University, 14 Belorusskaya St., Togliatti, 445020, Russia
[2]Institute for Metals Superplasticity Problems RAS, 39 S. Khalturin St., Ufa, 450001, Russia
[3]Department of Mechanical and Industrial Engineering, Norwegian University of Science and Technology, NTNU, Trondheim, N-7491, Norway

Magnesium and its alloys have several competitive advantages due to their low density and the highest specific strength among modern structural metallic materials. However, the relatively low ductility and poor corrosion resistance hinder their broader use in industry. Unlike many engineering applications, the ability of magnesium alloys to dissolve in chlorine-containing media is attractive for their applications as temporary implants. In the present work, the influence of thermomechanical processing on mechanical properties and corrosion resistance of the alloy Mg-1Zn-0.2Ca intended for biomedical applications is investigated. The low content of alloying elements permitted grain boundary hardening to be realised to a large extent during deformation processing. Severe plastic deformation through the multi-axis isothermal forging at relatively high homological temperatures in combination with isothermal rolling gave rise to the significantly refined to the micrometre scale homogeneous microstructure with an excellent balance of the tensile strength and ductility (the yield stress and ultimate tensile strength are in excess of 210 and 260 MPa, respectively, and the elongation at break is over 20%) and corrosion resistance in the simulated body fluid (SBF) *in vitro*. With the pH value of the SBF maintained at 7.4 throughout the test, the corrosion rate assessed by the hydrogen evolution and gravimetric methods was found to be nearly constant without signatures of saturation for the deformation-processed specimens. The rate of hydrogen desorption of 0.5 ml/cm^2/day was found to be far below the amount that could be accommodated by the human body without adverse effects.

Keywords: magnesium alloys, deformation processing, microstructure, mechanical properties, corrosion properties.

УДК: 669.0

Влияние деформационной обработки слаболегированного магниевого сплава Mg-1Zn-0.2Ca на механические свойства и скорость коррозии в биологически активной среде

Мерсон Д. Л.[†,1], Брилевский А. И.[1], Мягких П. Н.[1], Маркушев М. В.[2], Виноградов А.[3]

[1]Научно-исследовательский институт прогрессивных технологий, Тольяттинский государственный университет, ул. Белорусская, 14, Тольятти, 445020, Россия
[2]Институт проблем сверхпластичности металлов РАН, ул. С. Халтурина, 39, Уфа, 450001, Россия
[3]Кафедра механики и промышленных технологий, Норвежский университет естественных и технических наук, Трондхейм, N-7491, Норвегия

Магний и его сплавы обладают рядом конкурентных преимуществ благодаря низкой плотности и наивысшей среди современных структурных металлических материалов удельной прочности. Более широкому применению магниевых сплавов в промышленности мешают относительно низкая пластичность и плохая коррозионная стойкость. Улучшение этих свойств, при сохранении или даже повышении механической прочности, достигается за счёт прецизионного дизайна сплавов, определяющим в котором выступает химическая чистота, выбор легирующих компонентов и их концентрация. В отличие от многих инженерных приложений, способность

к растворению в хлорсодержащих средах является чрезвычайно привлекательной для применения магниевых сплавов в качестве временных имплантатов в биомедицинских приложениях. В настоящей работе исследовано влияние термомеханической обработки на механические свойства и сопротивление коррозии слабо-легированного сплава Mg-1Zn-0.2Ca, предназначенного для био-медицинских приложений. Слабое легирование сплава позволяет наиболее полно реализовать механизм зернограничного упрочнения и сформировать однородного микроструктуру в ходе деформационной обработки. Показано, что использование интенсивных пластических деформаций методом всесторонней изотермической ковки при относительно высоких гомологических температурах в сочетании с изотермической прокаткой позволяет значительно измельчить структуру литого сплава до микрометрического размера и получить превосходный баланс прочности и пластичности (предел текучести и предел прочности при растяжении превышают 210 и 260 МПа соответственно, а относительное удлинение при разрыве составляет более 20%), и коррозионной стойкости в искусственной физиологической среде *in vitro*. При поддержании значения pH среды на уровне 7.4 на протяжении всего испытания, скорость коррозии, оцененная с помощью выделения водорода и гравиметрического метода, оказалась почти постоянной без признаков насыщения для образцов после термо-механической обработки. Было установлено, что скорость десорбции водорода 0.5 мл/см^2/день намного ниже количества, которое может быть адаптировано человеческим организмом без каких-либо побочных эффектов.

Ключевые слова: магниевые сплавы, деформационная обработка, микроструктура, механические свойства, коррозионные свойства.

1. Introduction

With density in the range of 1.7 – 2.0 g/cm^3, magnesium alloys have the highest specific strength among structural metallic materials. This makes them very promising in industrial applications where weight reduction is of paramount importance. Other critical advantages of magnesium include, but not limited to, its excellent biocompatibility and the ability to dissolve gradually in biological media, which is important for manufacturing the temporary structures for bio-medical applications as implants [1] and vascular stents [2]. Not only the density of Mg-based alloys is very close to that of the cortical bone (1.8 to 2.0 gm/cm^3), but also their elastic modulus is in the range of 40 – 45 GPa which is far less than that of stainless steels (~200 GPa), Co-Cr alloys (~230 GPa), and Ti alloys (~110 GPa) — the materials dominating the implant market to date. Thus, the elastic response of magnesium is close to that of the bone (~30 GPa), which is very important to avoid or minimise stress shielding.

Despite an excellent balance between weight and strength, magnesium alloys have several disadvantages impeding their wider uptake. In the as-cast state, they have low strength and poor ductility, formability and corrosion resistance. These properties are generally improved by judicious alloying (often by rare-earth elements) and careful processing aiming at solid-solution strengthening and, chiefly, dispersion hardening with intermetallic particles of the second phases. Another strengthening strategy is based on grain refinement. However, magnesium alloys are hard to refine, especially to submicron and nano grain sizes [3], although these grain dimensions are readily achieved in many structural metals and alloys by the so-called severe plastic deformation (SPD) techniques [4]. Besides greain reinment, SPD processes are aimed at, redistributing/refining second phases, as well as controlling over the crystallographic texture. These measures collectively bring about the remarkable improvement of both strength and ductility of magnesium alloys [3]. The effect of SPD on the corrosion performance is, however, much less understood. Because of the high inherent reactivity of magnesium and little protection provided by the inherently porous and brittle surface corrosion magnesium oxide and hydroxide films, Mg alloys corrode relatively quickly in chloride-containing solutions [5]. While providing strength, the second phases particles accelerate corrosion significantly by micro-galvanic coupling between them and the surrounding metal matrix.

It has been frequently reported that grain size has a tremendous influence on the corrosion resistance of Mg alloys [6 – 8], and grain boundaries are often claimed as physical corrosion barriers, and smaller grain size led to better corrosion resistance [9]. Contradictory results, however, have been reported. On the one hand, grain refinement to the micrometre range induced by SPD led to better corrosion performance of various alloys [10 –15]. On the other hand, fine-grained pure Mg [16] and AZ91D [17] samples were found to be less corrosion resistant than their as-cast counterparts. Since the above-cited works refer to different alloys tested in different set-ups and media by different methods, it is difficult to draw conclusive comparisons between them. Therefore, the purpose of this paper is to evaluate the impact of different deformation processing schemes on the corrosion rate of the dilute Mg-Zn-Ca alloy, which is chosen to emphasize the grain boundary strengthening by deformation procedures and alleviate the significance of second phases in the corrosion behaviour.

2. Materials and Methods

The popular Mg-1Zn-0.2Ca (in wt.%) system, promising for biomedical applications due to its remarkable balance between the mechanical and corrosion properties [18] was investigated. The samples this alloy with nominally the same chemical composition were cast using commercially pure components. The chemical compositions of the obtained samples were assessed using the ARL 4460 optical emission spectrometer, and are given in Table 1.

The alloys were examined in four different conditions designated as follows:

- S11: the as-cast alloy was homogenised at 450°C for 12h in argon;

- S11V: state S11 was subjected to multi-axial isothermal forging (MIF) [19, 20] in the temperature range (400 – 300)°C

through 5 passes with 25°C temperature reduction after each pass;

- S11VP: state S11V followed by isothermal rolling (IR) at 300°C to the effective strain e ~0.84;

- J1: the alloy was two-step homogenised at 350°C for 12 h and 450°C for 8 h in argon and then direct extruded with a ratio of 5 at 350°C.

Microstructure examinations and surface profile measurements were carried out using the LEXT OLS4000 confocal laser scanning microscope. The specimens for metallographic investigations were obtained by mechanical grinding and polishing to of 0.25 μm grade using sandpaper and diamond suspensions. They were then etched in a solution containing 20 ml of distilled water, 75 ml of ethanol, 37.5 ml of acetic acid and 2 g of picric acid for 10 – 30 s.

Mechanical properties were evaluated using flat $10\times3\times4$ mm^2 specimens tested in tension on a screw-driven Kammrath&Weiss testing machine at 1×10^{-4} s^{-1} strain rate at room temperature in air.

The corrosion rate was measured by two independent methods — hydrogen evolution [21] and weight loss — on a series of three samples immersed in a simulated body fluid (SBF) for 168 hours in a thermostabilised at 37±1°C bath with 3 litres of slowly flowing SBF. A Ringer solution containing 8.6 g NaCl, 0.3 g KCl, 0.3 g $CaCl_2$ and 0.25 g $CaCl_2$-$6H_2O$ in 1 litre of distilled water was used as SBF. Since the human body maintains the pH nearly constant between 7.35 and 7.45, during the immersion test, the pH value was measured with an I-160MI pH-metre and automatically corrected to be 7.4 ± 0.4 using the correction solution containing 500 ml of Ringer SBF and 0.5 – 1 ml of orthophosphoric acid. Before testing, the samples with sizes $7\times7\times2$ mm^3 (alloy J1: $11\times5\times2$ mm^3) were ground to grade 2500 with sandpaper, rinsed in acetone using an ultrasonic bath, quickly fan-dried and weighed on an analytical scale with of 0.0001 g accuracy. After the immersion test, the corrosion products were removed by washing in a solution consisting of 200 g CrO_3, 10 g $AgNO_3$ and 1000 ml of distilled water. After removal the corrosion products, the samples were washed several times in ethanol, dried and weighed again.

3. Results and discussion

Fig. 1 shows optical images representing the typical grain structure of the specimens studied. The specimen S11 has a coarse-grained microstructure with relatively equiaxial grains (Fig. 1a), having average size of 185 μm (Table 2). Since all variants of the thermo-mechanical treatments were carried out at high homologous temperatures, the dynamic recrystallization (DRX) played a central role in the grain refinement [22, 23]. After MIF processing, the specimen S11V has a completely recrystallised structure (Fig. 1b), with average grain size of 2.9 μm (Table 2). Subsequent warm rolling (S11VR) led to even greater grain refinement down to ~2.2 μm (Table 2). The grains appear only slightly elongated in the rolling direction (Fig. 1c, d). For the extruded specimen J1, DRX is apparently uncompleted. A large volume fraction of initial heavily deformed grains (of 30 – 45 μm, Table 2) coexists with fine recrystallised grains of 4 – 7 μm in size (Table 2), leading to a bimodal grain size distribution. The fine DRX grains of a few-micrometre size nucleate primarily at stress risers close to the initial grain boundaries as is clearly visible for the specimen J1 in both extrusion (ED) and transverse directions (TD). The DRX process completes when the new grains replace the initial grains, and the

Table 1. Chemical compositions of the alloy Mg-1Zn-0.2Ca.

Sample	Mg	Zn	Ca	Zr	Y	Al	Fe	Cu	Ni	Si
S11	98.81	0.98	0.19	0.0027	< 0.001	0.0072	0.0021	0.0004	0.0016	0.002
J1	98.90	0.85	0.22	< 0.0001	< 0.001	0.0085	0.0072	0.0008	0.0014	0.007

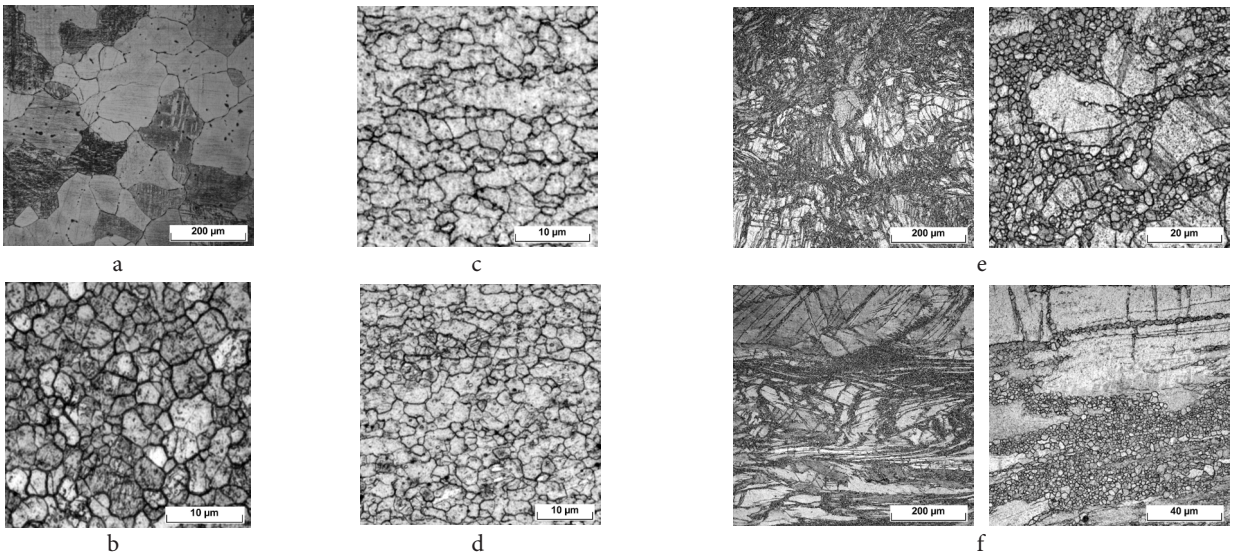

Fig. 1. Optical metallographic images showing the microstructure of the specimens tested: S11 (cast) (a), S11V (MIF) (b), S11VP direction ED (MIF+IR) (c), S11VP direction TD (MIF+IR) (d), J1 direction ED (extrusion) (e) and J1 direction TD (extrusion) (f). For J1 the microstructure is shown at two magnifications to highlight the difference in grain dimensions on different scales.

average grain size saturates as is seen in the MIF-processed specimens.

Due to a relatively low concentration of alloying elements, the volume fraction of the second phase is low. However, some relatively coarse intermetallic $Ca_2Mg_6Zn_3$ particles are visible in the as-cast alloy at the grain boundaries and in the grain interior (Fig. 1a) c.f. [24–26]. After hot extrusion of homogenised rods, this phase is practically not recognisable at optical magnification (Fig. 1e,f) yet it has been observed and identified in the similar alloys by transmission electron microscopy [27]. Even though it has been well understood that the significance of this phase in the mechanical and chemical performance of the Mg-Zn-Ca alloys cannot be overvalued, the details of the distribution of the $Ca_2Mg_6Zn_3$ phase in the microstructure and its evolution during processing are beyond the scope of this brief communication. Interested readers are encouraged to review the abovecited papers for details of this particular phase.

Table 2 shows the main tensile properties of the specimens studied. The specimen S11 in the homogenised condition exhibits a relatively high elongation at break, $\varepsilon_f = 22\%$, while its strength properties are low, c.f. the conventional yield stress $\sigma_{0.2}$ is as low as 37 MPa. MIF processing results in the remarkable enhancement of all mechanical properties: the yields stress is nearly tripled, reaching of 100 MPa, ultimate tensile strength σ_{UTS} increased by 20% to 200 MPa approximately, and the elongation at break improved by 14% up to 25%. Additional rolling results in the further notable increase in strength ($\sigma_{0.2} = 210$ MPa and $\sigma_{UTS} = 260$ MPa in the specimen S11VP) with only a small compromise in ductility reducing to $\varepsilon_f = 21\%$. The extrusion process (J1) gives rise to even better strength values reaching $\sigma_{0.2} = 235$ MPa and $\sigma_{UTS} = 285$ MPa, whereas the ductility is almost halved with $\varepsilon_f = 12\%$. Considering that only modest grain refinement has been archived through the extrusion process, the relatively high strength and compromised ductility are likely due to the known texture effects: a typical strong fibre prismatic texture is developed in Mg alloys after extrusion in which the *c*-axis aligns perpendicular to the extrusion direction, giving rise to the increased yield stress and reduced elongation to failure. This effect is relaxed in the course of MIF processing, resulting in a weaker texture [19,20]. Thus, of the investigated alloy variants, the best combination of mechanical properties is obtained after a combination of multiaxial forming and hot isothermal rolling in S11VP. Since this specimen possesses reasonably good ductility, the further enhancement of its strength is possible via additional rolling at the lower homologous temperature.

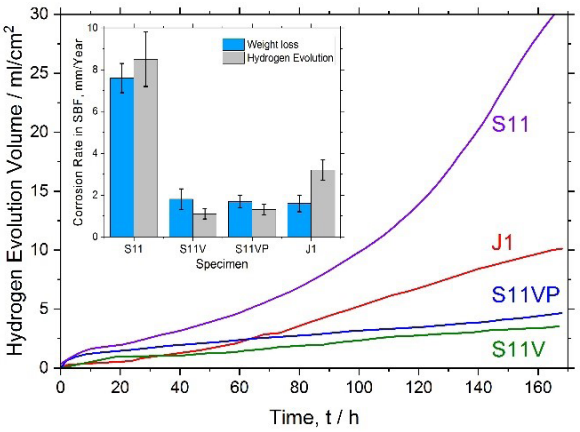

Fig. 2. (Color online) Hydrogen evolution curves for the magnesium alloy Mg-1Zn-0.2Ca in four different structural states tested in SBF for 168 hours. The inset compares the average corrosion rates estimated by the weight-loss and hydrogen evolution methods.

Fig. 2 shows the typical hydrogen evolution curves obtained upon immersion of the specimens in the Ringer SBF for 168 h. For convenient comparison with literature data, the corrosion rate is presented in both mm/year — the most common for the gravimetric method, and in ml/cm²/day — typical of the hydrogen evolution method. One can see that the deformation-processed specimens show a nearly steady corrosion rate with the almost linear hydrogen evolution in time. The behaviour of the as-cast alloy is different. Starting from approximately 20 hours, the hydrogen evolves with the progressively increasing rate. It should be noted that in all cases, hydrogen evolves faster in the first 8÷20 hours. This is due to more intense oxidation and formation of a layer of corrosion products on the initial ground surface.

General corrosion, pitting corrosion, and localised corrosion are known as the main corrosion mechanisms of magnesium alloys in SBF. Fig. 3 shows the appearance of the corroded samples and representative CLSM profilograms, illustrating the development of pits and the propagation of damage on the corroded surface. The general corrosion is not pronounced in the alloy studied. No signatures of intergranular corrosion were found. The same is frequently reported in the literature for Mg alloys where the corrosive attack does not propagate along grain boundaries, which are invariably cathodic relative to the grain matrix. However, pitting and localised corrosion develop on the surface in the grain interior of all specimens immersed in the SBF. The homogenised S11 specimens exhibited smaller and shallower pits, which tend to link up, and the number or density of which is notably higher than in other specimens

Table 2. Mechanical and corrosion properties of the alloy Mg-1Zn-0.2Ca after different deformation processing.

Sample	Processing	Yield stress, $\sigma_{0.2}$, MPa	Ultimate strength, σ_{UTS}, MPa	Elongation at break, ε_f (%)	Grain size, *D*, mm	Corrosion rate in SBF, mm/year		Average hydrogen evolution rate, ml/cm²/day
						Weight loss, P_m	Hydrogen evolution, P_H	
S11	As-cast	37±3	165±5	22±2	185±44	7.6±0.7	8.5±1.3	4.2±0.3
S11V	MIF	100±5	200±8	25±3	2.9±1.6	1.8±0.5	1.1±0.24	0.50±0.03
S11VP	MIF+IR	210±5	260±8	21±2	2.2±1.2	1.7±0.3	1.3±0.26	0.65±0.07
J1	Extrusion	235±6	285±10	12±1	5.2±1.6; 36±9.0	1.6±0.4	3.2±0.5	1.45±0.08

(see the profilogram in Fig. 3 a). Similar behaviour is characteristic of pure Mg. The initial pits in other samples tend to evolve to deep cavities. The most profound localised corrosion attack is systematically observed for the extruded J1 specimen, Fig. 3 d. The very deep and through-cavities may be attributed to the presence of occasional Fe-rich particles, which are hard to control, even if the amount of Fe is below the tolerance limit. Overall, all deformation-processed specimens exhibit strongly localised corrosion with deep cavities having similar lateral dimensions on the surface. This suggests that the corrosion process is electrochemical in nature and is caused by chemical heterogeneity of the specimens due to the presence of second phases. In contrast to the specimens S11V and S11VP, corrosion pits in the extruded specimen J1 are chain-linked, which is likely associated with the typical extrusion-induced elongated morphology of the grain microstructure, and inhomogeneous grain size distribution.

Possibly, in the deformation processed alloys, the initially nucleated corrosion pits grow in-depth with a relatively constant velocity while new corrosion sites do not nucleate at the surface. Therefore, the average corrosion rate remains practically constant throughout the test, with only a few deep cavities observed. For the S11 specimen, after the second day of exposure in the Ringer solution, concurrently with the stationary depth-wise growth of primary pits, the number of pits starts to increase, so that the corrosion rate increases steadily (Fig. 2).

Table 2 and the insert in Fig. 2 show the corrosion rate for all specimens tested by two methods: gravimetric and hydrogen evolution. The minimum corrosion rate of 1.5 mm/year is observed in the MIF-processed fine-grain specimens with the relatively uniform microstructure. This rate is approximately twice lower than that in extruded J1 and five times lower than in the as-cast alloy. The significant reduction in the corrosion rate after MIF can be associated with a collective effect of grain refinement and the reduced number of galvanic cells due to partial dissolution of the intermetallic phases into the matrix. The latter assumption has yet to be verified experimentally, and this is a scope of future research.

The excess emission of hydrogen gas during biosorption may give rise to the formation of subcutaneous gas pockets, which can adversely affect the healing process and induce complications such as superficial tissue necrosis and long term osteolytic lesions [28]. The remarkable result is that the hydrogen desorption rate in the S11V specimen was as low as 0.5 ml/cm^2/day (and slightly higher in S11VP), which that could be accommodated by the human body without any adverse effects (of 2.25 ml/cm^2/day limit according to [29,30]). On the other pole, the hydrogen evolution rate of the as-cast and homogenised specimen S11 was of 4 ml/cm^2/day, which is far beyond the tolerance limits in the human body.

The data presented in Table 2 and Fig. 3 allow a comparison to be made between the corrosion rates measured by weight loss, P_m, and the hydrogen evolution method, P_H. Both methods yield similar results. However, P_H was slightly less than P_m in S11V and S11VP specimens, which is consistent with the results reported in the literature in that P_H, was approximately linearly related to P_m in SBF with physiological p_H and temperature values [31] but was consistently lower. The observed difference between P_H and P_m is commonly attributed to the partial dissolution of hydrogen in the Mg matrix. This suggestion, however, has yet to be verified experimentally with care. The recent results using the thermo-desorption gas analysis applied to pure Mg, ZK60 and AZ31 alloys after several hours of immersion in the NaCl solution [32] showed that the concentration of diffusible hydrogen was negligible. The corrosion rate assessed by the gravimetric method was found smaller in the specimens S11 and J1; note that the difference between P_H and P_m in J1 is of 50%. This is not in line with the commonly observed trends. In principle, the weight loss method can generate such inconsistency associated with a procedure for removing corrosion products. The foremost consideration in this procedure is that removal must be complete, which is not necessarily guaranteed and which is hard to control for the severely corroded surfaces with deep cavities.

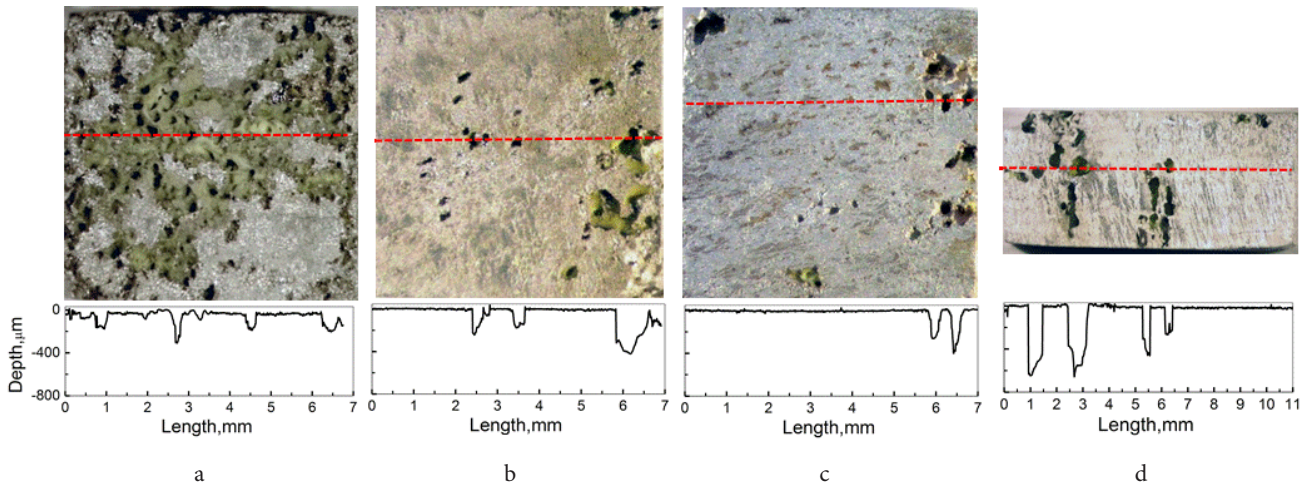

Fig. 3. (Color online) CLSM microscopy images showing the corroded surface of the Mg-alloy samples after immersing in Ringer SBF for 168 h; corresponding profiles obtained along the dashed lines after removal of corrosion products are shown on the bottom line: S11 (cast) (a), S11V (MIF) (b), S11VP (MIF+IR) (c) and J1 (extrusion) (d).

4. Conclusions

The deformation processing of the biodegradable Mg-1Zn-0.2Ca alloy, including MIF followed by warm rolling, allows obtaining an excellent balance between the strength, ductility and corrosion resistance.

The deformation processing resulting in the refined microstructure sharply reduces the number of corrosion nucleation sites and, therefore, reduces the average corrosion rate. The corrosion process is dominated by localised pit formation and depth-wise growth. The deformation processing affects this process to some extent, but it does not alter the overall picture.

After the first hours of immersion in the SBF (8 ÷ 20 hours) when the initial protective layer forms and when the accelerated corrosion attack occurs, the corrosion rate stabilises and proceeds nearly linearly for days.

The remarkable result is that the hydrogen evolution rate in all deformation-processed fine-grain Mg-1Zn-0.2Ca specimens (increased in the order MIF- > MIF + IR-ZExtrusion) was low enough to eliminate the adverse effects from hydrogen gas accumulation in the human body in the course of bio-degradation.

Acknowledgements. This research was funded by the Ministry of Education and Science of the Russian Federation under the contract RFMEFI58317X0070. Special thanks go to Prof. Y. Kawamura, Magnesium Research Center, Kumamoto University, Japan, for providing the materials for this study.

References

1. F. Witte, N. Hort, C. Vogt, S. Cohen, K.U. Kainer, R. Willumeit, F. Feyerabend. Current Opinion in Solid State and Materials Science. 12, 63 (2008). Crossref
2. M. Moravej, D. Mantovani. International Journal of Molecular Sciences.12, 4250 (2011). Crossref
3. A. Vinogradov, V.N. Serebryany, S.V. Dobatkin. Advanced Engineering Materials. 20, 1700785 (2018). Crossref
4. Y. Estrin, A. Vinogradov. Acta Materialia. 61, 782 (2013). Crossref
5. A. Atrens, G.-L. Song, M. Liu, Z. Shi, F. Cao, M.S. Dargusch. Advanced Engineering Materials. 17, 400 (2015). Crossref
6. H. Wang, Y. Estrin, H. Fu, G. Song, Z. Zúberová. Advanced Engineering Materials. 9, 967 (2007). Crossref
7. K.D. Ralston, N. Birbilis, C.H.J. Davies. Scripta Materialia. 63, 1201 (2010). Crossref
8. Z. Pu, G.L. Song, S. Yang, J.C. Outeiro, O.W. Dillon, D.A. Puleo, I.S. Jawahir. Corrosion Science. 57, 192 (2012). Crossref
9. N.N. Aung, W. Zhou. Corrosion Science. 52, 589 (2010). Crossref
10. M. Alvarez-Lopez, M.D. Pereda, J. A. del Valle, M. Fernandez-Lorenzo, M.C. Garcia-Alonso, O.A. Ruano, M.L. Escudero. Acta Biomaterialia. 6, 1763 (2010). Crossref
11. N. Birbilis, K.D. Ralston, S. Virtanen, H.L. Fraser, C.H. J. Davies. Corrosion Engineering, Science and Technology. 45, 224 (2010). Crossref
12. P. Minárik, R. Král, M. Janeček, F. Chmelík, B. Hadzima. Acta Physica Polonica A. 128, 772 (2015). Crossref
13. D. Orlov, K.D. Ralston, N. Birbilis, Y. Estrin. Acta Materialia. 59, 6176 (2011). Crossref
14. E.V. Parfenov, O.B. Kulyasova, V.R. Mukaeva, B. Mingo, R.G. Farrakhov, Y.V. Cherneikina, A. Yerokhin, Y.F. Zheng, R.Z. Valiev. Corrosion Science. 163, 108303 (2020). Crossref
15. N.S. Martynenko, E.A. Lukyanova, V.N. Serebryany, M.V. Gorshenkov, I.V. Shchetinin, G.I. Raab, S.V. Dobatkin, Y. Estrin. Materials Science and Engineering A. 712, 625 (2018). Crossref
16. D. Song, A. Ma, J. Jiang, P. Lin, D. Yang, J. Fan. Corrosion Science. 52, 481 (2010). Crossref
17. D. Song, A.B. Ma, J.H. Jiang, P.H. Lin, D.H. Yang, J.F. Fan. Corrosion Science. 53, 362 (2011). Crossref
18. J. Hofstetter, E. Martinelli, S. Pogatscher, P. Schmutz, E. Povoden-Karadeniz, A.M. Weinberg, P.J. Uggowitzer, J.F. Löffler. Acta Biomaterialia. 23, 347 (2015). Crossref
19. D.R. Nugmanov, O.S. Sitdikov, M.V. Markushev. Letters on Materials. 1 (4), 213 (2011). (in Russian) [Д.Р. Нугманов, О.Ш. Ситдиков, М.В. Маркушев. Письма о материалах. 1 (4), 213 (2011).] Crossref
20. M.V. Markushev, D.R. Nugmanov, O. Sitdikov, A. Vinogradov. Materials Science and Engineering A. 709, 330 (2018). Crossref
21. G. Song, A. Atrens, D. StJohn. An Hydrogen Evolution Method for the Estimation of the Corrosion Rate of Magnesium Alloys. In: Essential Readings in Magnesium Technology (Ed. by S.N. Mathaudhu, A.A. Luo, N.R. Neelameggham, E.A. Nyberg, W.H. Sillekens). Springer (2016) pp. 565 – 572.
22. R. Kaibyshev. Dynamic recrystallization in magnesium alloys. In: Advances in Wrought Magnesium Alloys. Woodhead Publishing (2012) pp. 186 – 225. Crossref
23. A. Galiyev, R. Kaibyshev, G. Gottstein. Acta Materialia. 49, 1199 (2001). Crossref
24. H.R. Bakhsheshi-Rad, E. Hamzah, A. Fereidouni-Lotfabadi, M. Daroonparvar, M.A.M. Yajid, M. Mezbahul-Islam, M. Kasiri-Asgarani, M. Medraj. Materials and Corrosion. 65, 1178 (2014). Crossref
25. B. Zhang, Y. Hou, X. Wang, Y. Wang, L. Geng. Materials Science and Engineering C. 31, 1667 (2011). Crossref
26. A. Vinogradov, E. Vasilev, M. Linderov, D. Merson.Metals. 6, 304 (2016). Crossref
27. J. Hofstetter, S. Rüedi, I. Baumgartner, H. Kilian, B. Mingler, E. Povoden-Karadeniz, S. Pogatscher, P.J. Uggowitzer, J.F. Löffler. Acta Materialia. 98, 423 (2015).Crossref
28. Y.-K. Kim, K.-B. Lee, S.-Y. Kim, K. Bode, Y.-S. Jang, T.-Y. Kwon, M.H. Jeon, M.-H. Lee. Science and Technology of Advanced Materials. 19, 324 (2018). Crossref
29. H.R. Bakhsheshi-Rad, E. Hamzah, M. Daroonparvar, R. Ebrahimi-Kahrizsangi, M. Medraj. Ceramics International. 40, 7971 (2014). Crossref
30. C.-Y. Zhang, R.-C. Zeng, C.-L. Liu, J.-C. Gao. Surface and Coatings Technology. 204, 3636 (2010). Crossref
31. S. Johnston, Z. Shi, A. Atrens. Corrosion Science. 101, 182 (2015). Crossref
32. E. Merson, P. Myagkikh, V. Poluyanov, D. Merson, A. Vinogradov. Materials Science and Engineering A. 748, 337 (2019). Crossref